Title

Ambient gas effects on the dynamics of laser-produced tin plume expansion

Journal

Journal of Applied Physics, 99

Authors

Harilal, S S

O'Shay, B

Tillac, M S

et al.

Publication Date

2006

Peer reviewed

Ambient gas effects on the dynamics of laser-produced tin plume expansion

S. S. Harilal,[a] Beau O'Shay, Yezheng Tao, and Mark S. Tillack
Center for Energy Research, University of California San Diego, 9500 Gilman Drive, La Jolla, California 92093

(Received 27 September 2005; accepted 8 February 2006; published online 28 April 2006)

Controlling the debris from a laser-generated tin plume is one of the prime issues in the development of an extreme ultraviolet lithographic light source. An ambient gas that is transparent to 13.5 nm radiation can be used for controlling highly energetic particles from the tin plume. We employed a partial ambient argon pressure for decelerating various species in the tin plume. The kinetic energy distributions of tin species were analyzed at short and large distances using time and space resolved optical emission spectroscopy and a Faraday cup, respectively. A fast-gated intensified charged coupled device was used for understanding the hydrodynamics of the plume's expansion into argon ambient. Our results indicate that the tin ions can be effectively mitigated with a partial argon pressure ~65 mTorr. Apart from thermalization and deceleration of plume species, the addition of ambient gas leads to other events such as double peak formation in the temporal distributions and ambient plasma formation. © *2006 American Institute of Physics*. [DOI: 10.1063/1.2188084]

I. INTRODUCTION

Currently there is a lot of effort going into the development of a clean and powerful source at 13.5 nm for extreme ultraviolet lithography (EUVL).[1,2] The wavelength of choice is based on the availability of Mo/Si multi-layer mirrors that reflect more than 70% of the in-band radiation centered at 13.5 nm with 2% bandwidth. Laser generated plasmas from xenon,[3] lithium,[4] and tin[5] are considered to be strong candidates for an EUVL light source. One of the most important problems encountered with a laser-produced plasma source for EUVL is the debris from the plume. In general, the debris from laser-generated plasma can include energetic ions, neutrals, particulates, and molten droplets. In an EUVL tool, the collector mirror is expected to be placed ~15–20 cm from the plasma source. For industrializing EUVL, a lifetime of more than 10^9 shots is needed for the collector mirror. So controlling the debris from laser plasma is the most important task for creating a clean photon source for EUVL. Being an inert gas, laser-produced plasmas from xenon act as a particulate free source, but reported conversion efficiency from xenon is less than 1%.[6] Laser-produced tin plasma is more promising in this context as it provides a higher conversion efficiency than xenon based targets.[7] Conventional solid metal targets, however, can pose extreme debris problems in commercial lithography processes.[8–10] Mitigation of the debris has been attempted using various methods including tape targets,[11] mass limited droplet targets,[12] the application of electrostatic repeller fields,[10] and magnetic fields.[9] An ambient gas can also be used as a stopper for highly energetic tin ions.

The use of an ambient gas environment for controlling highly energetic particles from a tin plume can be an effective way to mitigate debris. This is a standard method used in pulsed laser deposition (PLD), where ambient gas species act as a moderator for the energetic plume species during the flight time from target to substrate.[13,14] Flora *et al.*[15] and Bollanti *et al.*[16] used krypton for controlling debris from a laser-produced Ta plasma and their results showed that the ambient gas significantly reduced the debris at the witness plate. However, a systematic study on the effect of ambient gas on tin plasma dynamics is still lacking. The plume expansion into vacuum is adiabatic[17] and treated well by Anisimov *et al.*[18,19] and Narayan and co-workers.[20,21] Compared to the expansion into vacuum, the interaction of the plume with an ambient gas is a far more complex gas dynamic process that involves deceleration, attenuation, and thermalization of the ablated species, as well as the formation of shock waves.[22–27] Recent measurements performed over a wide range of expansion durations have demonstrated a fairly complicated gas dynamic picture of plume ambient gas interaction. This is characterized by different propagation phases and is accompanied by plume oscillations arising at rather high background pressures.[28,29] Still, a comprehensive modeling analysis of the expansion dynamics of the laser-ablated plume in an ambient is missing because of the many complex nonlinear processes occurring during the expansion.

It is well known that most gases absorb EUV radiation around 13.5 nm even at moderate pressures. So care must be taken in selecting a proper ambient environment for an EUVL source setup. Hydrogen, helium, and argon gases provide exceptionally good transmission to 13.5 nm compared to other gases. Being lighter in mass, a hydrogen or helium ambient environment may require higher pressures to control energetic tin ions and other particulates emanating from a laser-produced tin plasma. At a particular pressure, being heavier, argon (atomic weight=40 amu) is expected to be more effective for slowing down the energetic ions and atoms in comparison with hydrogen or helium ambient. Because of this reason we used argon gas as an ambient for controlling the various species from the tin plasma. The pho-

[a]Electronic mail: harilal@fusion.ucsd.edu

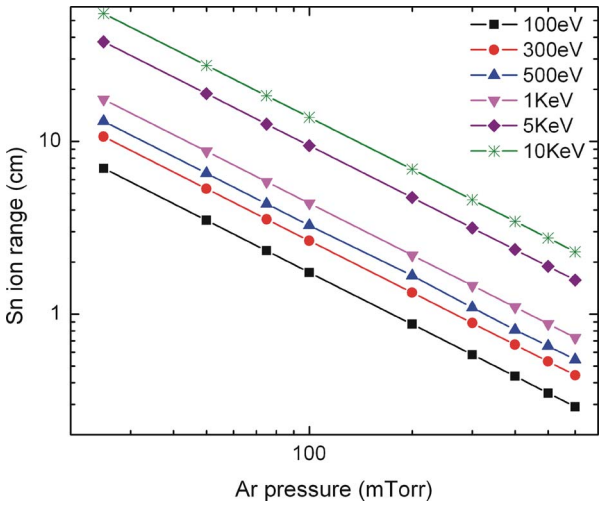

FIG. 1. (Color online) The theoretical calculation of the flight range of tin ions with different values of initial energies propagating into an argon ambient gas. These estimates were made using the SRIM code.

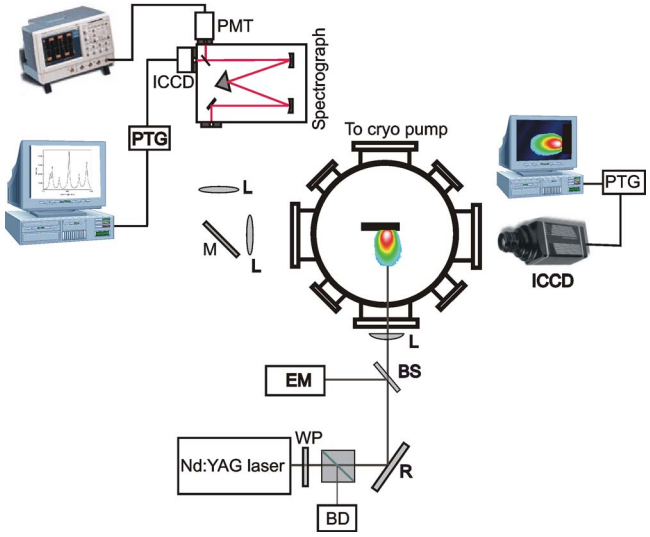

FIG. 2. (Color online) Schematic of the experimental setup used for space and time resolved optical emission spectroscopy of tin plume and ICCD imaging. (WP, wave plate; BD, beam dump; BS, beam splitter; L, lens; EM, energy meter; R, reflector; M, mirror, and PTG, programmable timing generator).

toabsorption cross section for argon at 13.5 nm is 2.08×10^4 cm^2/g.[30] X-ray transmission studies showed that more than 90% of the 13.5 nm radiation is transmitted for a path length of 20 cm when the argon pressure is less than 120 mTorr.[31]

The mass stopping power S in its simplest notation based on Bethe-Bloch formula can be written as[32]

$$S = \frac{kZ_2}{\beta^2} Z_1^2 L_\beta, \tag{1}$$

where Z_1 and Z_2 are the atomic numbers of projected species and target atoms, respectively; β, the relative particle velocity (v/c); $k=0.3071/M_2$ and having a unit of keV/(mg/cm^2), where M_2 being the mass of the target, and L_β is the dimensionless "stopping number." The stopping number is expressed in power series of Z_1 and used for adding corrections to the basic two-particle energy loss process and k represents the energy loss per mg/cm^2 of the target transited. An estimate was made of the mean projected length of tin ions at different argon ambient pressures based on the popular Monte Carlo simulation program the stopping range of ions in matter (SRIM).[33,34] Figure 1 shows the theoretical calculation of the flight range of tin ions with different values of starting energies propagating into an argon ambient gas with various pressure levels. It shows that with a 100 mTorr argon pressure, the ions with kinetic energies $\leqslant$5 keV can be effectively stopped before reaching the collector mirror. The flight range estimations with helium and hydrogen gases showed that a helium pressure of about 625 mTorr and a hydrogen pressure of 775 mTorr are necessary to provide similar stopping power obtained with 100 mTorr of argon. Under these pressure conditions helium is found to be more absorptive to 13.5 nm radiation than argon at 100 mTorr. In fact, hydrogen at 775 mTorr is more transparent to in-band radiation than 100 mTorr argon. But being heavier in mass, argon is expected to control heavier cluster debris from the tin plasma than hydrogen ambient. A comparative experimental study with argon, helium, or hydrogen as buffer gas is necessary to obtain more insight in this context.

In this paper, time and space resolved optical emission spectroscopy is employed to reveal the velocity distribution of different species ejected during tin laser ablation in the presence of argon ambient at distances up to 25 mm from the target surface. Such temporally and spatially resolved high resolution spectroscopic studies are helpful for understanding the evolution of the tin plume in the presence of an ambient gas. The kinetic distributions of ions and electrons at greater distances are studied using a Faraday cup. Our results indicate that energetic tin ions emanating from the plume can be stopped with a partial argon pressure of ~100 mTorr. However, the insertion of an ambient gas leads to the creation of ambient plasma. This is caused by the collisional excitation and ionization of ambient gas species when it interacts with transient expanding plasma. Temporal profiles of ambient plasma species were recorded to characterize the mechanism involved in the ambient gas excitation and ionization. We also utilized two-dimensional (2D) gated photography for studying the spatial behavior of the tin plasma expansion into an argon buffer ambient.

II. EXPERIMENTAL DETAILS

The schematic of the experimental setup is given in Fig. 2. 1064 nm, 10 ns [full width at half maximum, (FWHM)] pulses from a Nd:yttrium aluminum garnet (YAG) laser were used to create tin plasma in a stainless steel vacuum chamber. The vacuum chamber was pumped using a cryogenic pump and a base pressure of $\sim 10^{-6}$ Torr was easily achieved. The laser beam, at normal incidence, was focused onto the target using a plano-convex lens to a focal spot diameter of 60 μm. The focal spot at the target surface was measured using an optical imaging technique and remained unchanged during the experiment. A 2 mm thick tin target in the form of a slab was translated to provide a fresh surface

for each shot to avoid errors associated with local heating and drilling. The beam energy was monitored using a thermal surface absorbing energy meter (Ophir, Model 30A).

The light emitted from the luminous plasma was transmitted though a quartz window mounted orthogonally to the direction of plume expansion. An optical system was used to image the plasma plume onto the entrance slit of a 0.5 m Czerny-Turner spectrograph (Acton Pro, Spectra-Pro 500i) so as to have one-to-one correspondence with the sampled area of the plume and the image. By translating the optical system along the direction of target normal, spatiotemporal information about the plume's emission could be detected. One of the exit ports of the spectrograph was coupled to an intensified charged coupled device (ICCD) (PI MAX Model 512 RB) and the other exit port was coupled to a photomultiplier tube (PMT). The ICCD was operated with vertical binning of the CCD array to obtain spectral intensities versus wavelength. A programmable timing generator (PTG) was used to control the delay time between the laser pulse and the detector system with an overall temporal resolution of 1 ns. The spectrograph was equipped with three gratings: 150, 600, and 2400 g/mm. The effective dispersions with 150, 600, and 2400 grooves/mm were 12.6, 3.1, and 0.6 nm/mm, respectively. For time resolved studies of a particular species in the plume, the specific emission lines were selected by tuning the grating and imaging onto the slit of the PMT. Recording the temporal profiles was accomplished by coupling the output of the PMT to a 500 MHz digital phosphor oscilloscope (5 GS/s, Tektronics TDS 5054B-NV). The ion and electron emissions have been also monitored using a Faraday cup (Kimball Physics Inc.) placed at a distance of 15 cm from the target surface and at an angle approximately 12° with respect to the target normal. The ion and electron currents were measured by acquiring the voltage signal across a load resistor by a 500 MHz digital phosphor oscilloscope.

Plume imaging was accomplished with an ICCD camera placed orthogonal to the laser beam. A Nikon lens was used to image the plume region onto the camera to form a two-dimensional image of the plume intensity. The visible radiation from the plasma was recorded integrally in a wavelength range of 350–900 nm.

III. RESULTS AND DISCUSSION

A. Time of flight studies

Optical emission spectroscopic studies showed that most of the species emitted by laser-produced tin ablation plumes in the present experimental conditions are singly ionized tin species along with excited neutrals.[35] Although the dominant species during EUV emission are Sn^{8+}–Sn^{13+}, recombination reduces the charge state significantly in the late-stage plume evolution. To elucidate the influence of an ambient gas environment on various species in the plasma plume, time of flight (TOF) profiles were taken at different distances from the target surface. TOF studies of the plume give vital information regarding the time taken by a particular state of the constituent to evolve after the onset of plasma. This technique gives details on the velocity and hence kinetic energy

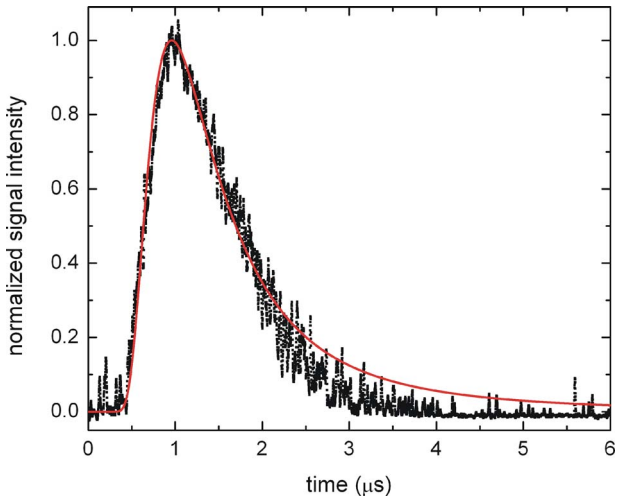

FIG. 3. (Color online) Intensity variation of spectral emission with time for Sn species (317.5 nm, $5p6s\ ^3P_1{}^0-5p\ ^{23}P_2$) recorded at 7 mm from the target surface. The measurements were done in vacuum and a laser power density of 4×10^{11} W cm^{-2} was used. The solid line represents a SMB fit. (The fitting parameters are $\nu_0=150$ m/s, $kT=36$ eV).

of the emitted particles and parameters that are of fundamental importance in establishing the mechanisms responsible for the particle emission.[36,37] Optical TOF profiles of various transitions at 335.2 nm (Sn^+, $5p^2\ ^2D$-$3f^2F^0$) and 317.5 nm (Sn, $5p6s^3P_1{}^0-5p^{23}P_2$) at different distances from the target surface were investigated. TOF data often can be represented by a shifted Maxwell-Boltzmann (SMB) distribution with a center of mass shifted streaming velocity given by[13]

$$f(\nu)=A\left(\frac{m}{2\pi k}\right)^{3/2}\nu^3 e^{-m(\nu-\nu_0)^2/2kT}d\nu, \tag{2}$$

where A is the normalization parameter, ν and ν_0 are the velocities of the species and center of mass velocity, T is the translational temperature, k is the Boltzmann constant, and m is the mass of the species. The SMB distribution assumes that the speed distribution has equilibrated after propagating a short distance from the target surface, and that the signal is a direct measure of the concentration of the indicated species. Figure 3 gives the TOF profile recorded for Sn species at 7 mm from the target surface in vacuum. A laser irradiance of 4×10^{11} W cm^{-2} was used for all measurements. The selection of this laser irradiance is based on the fact that our EUV spectroscopic studies showed the unresolved transition array (UTA) around 13.5 nm from tin plasma to peak at this intensity level using a 60 μm spot size.[38] The figure indicates that the SMB fit is in relatively good agreement with the experimental observed TOF curve.

The addition of ambient gas usually affects the kinetic distribution of all species in the plume because of plume-buffer interactions. Gas phase collisions can transform the initial temporal distributions into a very different final distribution. Typical TOF profiles recorded for Sn^+ and Sn at various locations in the plume in a direction perpendicular to the target surface at an argon pressure of 100 mTorr are given in Figs. 4 and 5, respectively. The time evolution of the spectral emission profiles obtained at 100 mTorr of argon clearly reveals that the Sn^+ species ejected by the tin plume exhibits a

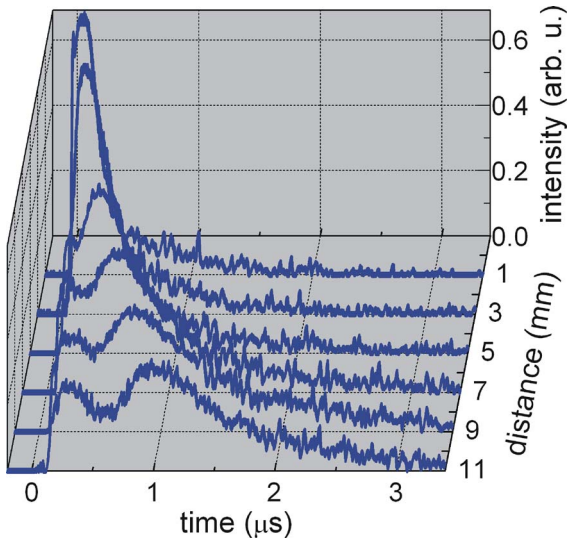

FIG. 4. (Color online) Representative emission TOF profiles recorded for Sn^+ (335.2 nm, $5p^2\,{}^2D$-$3f^2F^0$) at various locations in the plume in a direction perpendicular to the target surface at an argon pressure of 100 mTorr.

twin-peak TOF distribution. The twin-peak distribution is observed only beyond a certain distance from the target. At distances very close to the target surface (<4 mm) the temporal profiles are characterized by a single peak distribution. The reason for the occurrence of a twin peak will be discussed in the later sections.

The *R-t* (distance-time) plots drawn for Sn and Sn^+ species recorded in vacuum and 100 mTorr argon pressure are given in Fig. 6 (Pk1 and Pk2 are designated as faster and slower Sn^+ peaks). For obtaining a *R-t* plot, the time corresponding to peak signal intensity is used. In vacuum, the arrival time of both neutral and ionic species exhibited a nearly linear dependence over the whole range of distances for which emission could be detected. The estimated expansion velocities of the Sn^+ and Sn species were $1.8\pm0.1\times10^6$ cm/s (200 eV) and $8\pm0.3\times10^5$ cm/s (40 eV) in

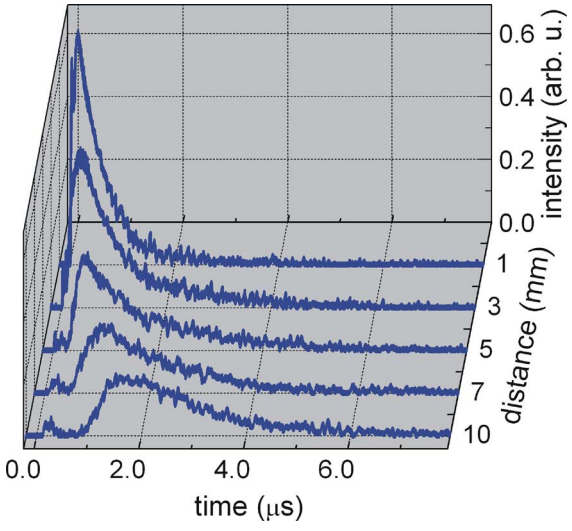

FIG. 5. (Color online) Typical TOF emission profiles recorded at various distances from the target for excited Sn species (317.5 nm, $5p6s\,{}^3P_1{}^0$–$5p\,{}^{23}P_2$). A background argon pressure of 100 mTorr was used for these measurements.

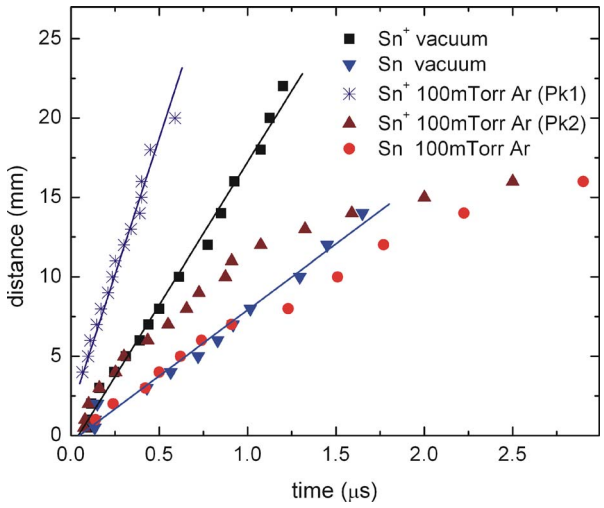

FIG. 6. (Color online) The *R-t* plots obtained from TOF profiles of Sn and Sn^+ species recorded for vacuum and 100 mTorr argon pressure. The plume expansion into vacuum followed $R\propto t$ relation. With 100 mTorr argon pressure, the Pk2 of Sn^+ followed approximately $R\propto t^{0.54}$ and Sn species followed $R\propto t^{0.7}$, respectively, while the Pk1 of Sn^+ also found to vary linearly with time.

vacuum. In a laser-produced plasma, the ions typically have higher kinetic energies than neutrals, since their expansion is influenced by the space charge effect in addition to pressure gradients.[39] The presence of energetic neutrals was also observed in the plume due to recombination of energetic ions.[40] The addition of ambient gas can affect the dynamics of various species in the plume. With increasing pressure, due to the enhanced collision with the background gas species, slowing of the plume species occurs. Thus, the ambient gas acts as a retarding medium, slowing the plume development and bringing the ion energy closer to the energy of excited neutral atomic species in the plasma. In the presence of 100 mTorr of argon, Pk1 and Pk2 of Sn^+ followed $R\propto t$ and $R\propto t^{0.54}$ dependence, while the neutral Sn species followed $R\propto t^{0.78}$.

In vacuum, the temporal profiles of Sn^+ species are described by a single peak distribution. In the presence of the ambient gas, the dynamics of the plume is governed by the nature and pressure of the buffer gas. *R-t* plots obtained from TOF profiles (Fig. 6) indicate that at 100 mTorr argon pressure, the kinetic properties of both Sn^+ (Pk2) and Sn species are largely affected at distances $\geqslant$6 mm. It shows at shorter distances that the plasma pressure is so high that the background gas species have a negligible effect on the plume expansion dynamics. The deceleration begins when the plume dimensions become comparable with the mean free path (mfp) of the ablated species. (mfp ~4 mm estimated using the equation given in Ref. 11). Based on the modeling of Westwood[41] of the scattering of sputter atoms by an ambient gas, a Sn atom in collision with an argon atom changes its direction by ≈16° and loses ≈40% of its kinetic energy.

The estimated stopping distance using SRIM for Sn ions at 100 mTorr with an initial energy of 200 eV showed 2.24 cm. The *R-t* plot of Pk2 of Sn^+ as well as Sn species showed stagnation tendency when the distance is greater than 15 mm. It should be remembered that SRIM does not

consider the collision of the plasma. So the effective experimental stopping distance may be different compared to SRIM analysis. It is interesting to note that Pk1 of Sn^+ species observed with 100 mTorr argon pressure propagates without much attenuation. It shows that these species penetrate into the ambient environment without loosing their energy. The estimated expansion velocity of fast moving Sn^+ species is $3.2\pm0.1\times10^6$ cm/s which corresponds to a kinetic energy of 650 eV.

We observed a peculiar double peak structure in the temporal profiles of the Sn^+ species. The dual peak structure is observed only above a certain distance from the target surface (>4 mm). In fact, the occurrence of multiple peak structures in TOF emission profiles is not new and was observed previously by several groups and discussed thoroughly in the literature.[37,42–45] We recently reported plume splitting in a laser created aluminum plasma expanding into an ambient air environment where gas phase collisions transformed the initial temporal distribution into a very different final distribution.[29] We distinguished three distinct pressure regimes using fast photography, each of which is characterized by particular behavior of the plume. At low pressure or in vacuum, the plume expands freely without any external viscous force. At intermediate pressure levels (transition regime), the plume is characterized by strong interpenetration of the plasma species and background gas that leads to plume splitting and sharpening[28] and at high-pressure levels, the plume eventually stops and particles become thermalized. Recently, Amoruso *et al.*[25] also identified three similar pressure regimes experimentally and Itina *et al.*[26] numerically studied this phenomenon. In the transition regime a part of the plume penetrated into the ambient gas with vacuum-like expansion and another division of the plume species decelerated after interaction with ambient gas that lead to plume splitting.

The plume splitting phenomena were first observed by Geohegan[46] and Geohegan and Puretzky[47] in laser-produced ytrrium barium copper oxide (YBCO) plasma expansion into oxygen ambient and later Wood *et al.*[48] explained these phenomena based on a combination of multiple elastic scattering and hydrodynamic formulations.

In the present experiment, the presence of ambient gas initiated a faster component of Sn^+ that were found to move with much higher velocities than plume expansion into vacuum. Usually, plume splitting behavior is characterized by the occurrence of a delayed component which appears at higher-pressure levels above a specific distance whose dynamics are strongly dependent upon the pressure of the ambient gas.

In order to check more aspects of the double peak formation and its pressure dependence, temporal profiles of Sn and Sn^+ were recorded at different argon pressure levels. Representative TOF profiles for Sn^+ species recorded at a distance of 10 mm from the target for various argon pressures are shown in Figs. 7(a) and 7(b). With increasing pressure, the lifetime of all the species increases as evidenced by a long tail. At low pressures or in vacuum the temporal profiles of Sn^+ species are described by a single peak distribution. As the pressure increases, the temporal distribution of

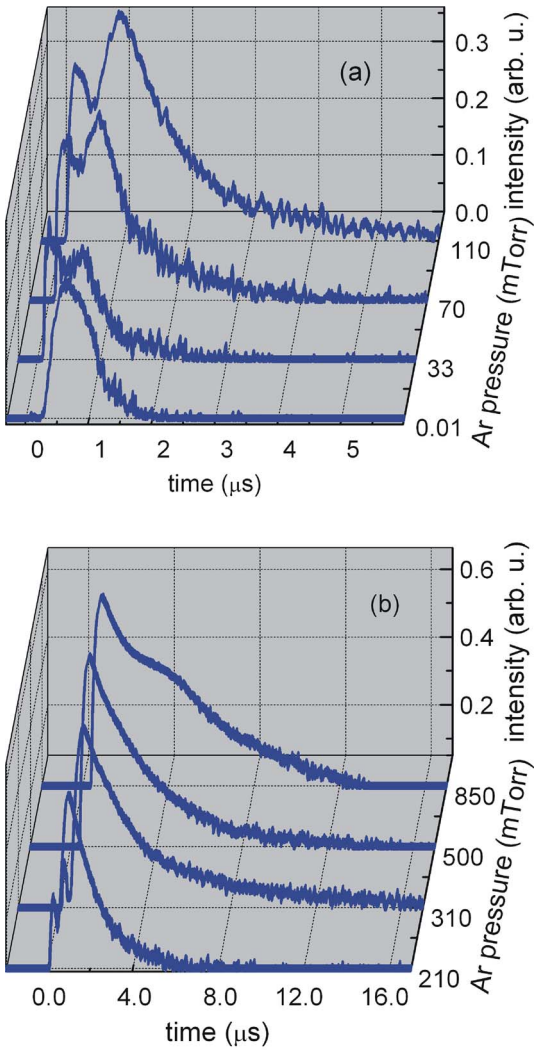

FIG. 7. (Color online) Representative TOF profiles for Sn^+ species recorded at a distance of 10 mm from the target for various argon pressures are given.

excited Sn^+ changed to a twin-peak distribution. With increasing pressure the arrival time of the delayed peak increases while the intensity of the faster peak drops and disappears above certain pressure levels. Hence the double peak distribution existed only in a pressure range (30–300 mTorr). It indicates that argon ambient plays an important role in the formation of the faster peak.

Variation of time delay for the peaks Pk1 and Pk2 of Sn^+ along with Sn species with respect to argon ambient gas pressure (distance of 10 mm) is given in Fig. 8. It shows that the excited neutral Sn and slower peak of Sn^+ species move with a constant velocity until the pressure ~60 mTorr while the braking effect of the ambient gas starts above this pressure range. It must be remembered that these properties strongly depend upon the distance from the target surface. At high pressures, due to enhanced collisions with the background gas species, the deceleration process is very rapid. We also noticed that at larger pressures (>600 mTorr) the decay of the Sn^+ species transformed into other delayed components showing plume splitting phenomena. Plume splitting phenomena in the presence of high background gas pressures, as described previously, have been seen and reported

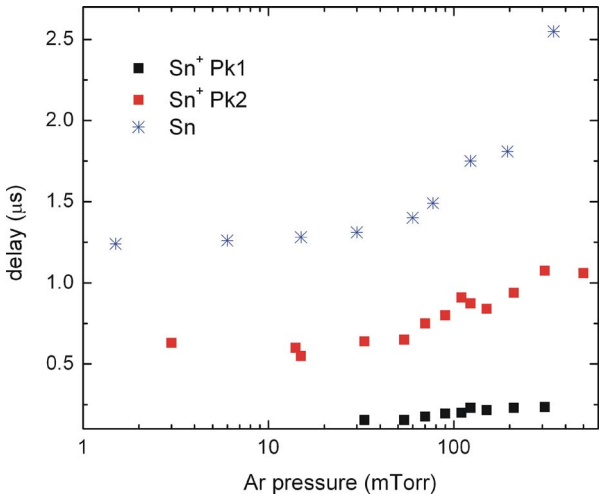

FIG. 8. (Color online) Variation of time delay for the peaks Pk1 and Pk2 of Sn^+ along with Sn species with respect to argon ambient gas pressure is given. All the measurements were done at a distance of 10 mm from the target.

by several groups.[42,45] This happens when a collection of species escapes without much collision with ambient gas and the bulk of the species undergoes numerous collisions and hence decelerates to form a delayed component.

With 100 mTorr argon, most of the species in the plume were considerably slowed down even within 25 mm from the target surface. But we need to know the kinetic energy distributions of the ions at distances ~15 cm from the target where the collector mirror is expected to be placed in an EUVL setup. Since most of the plume species are not emitting at large distances, optical TOF emission is not a valuable diagnostic tool for measuring kinetic distributions at distances greater than 25 mm. A Faraday cup or electrostatic analyzer should be useful for measuring the kinetic energies of various species at higher distances.

We utilized a Faraday cup for measuring the kinetic distributions of tin ions. The Faraday cup is placed ~15 cm away from the target surface and at an angle approximately 12° with respect to the target normal. Typical TOF profiles recorded at the collecting plate are given in Fig. 9 for tin ions in vacuum and 100 mTorr argon pressures. The kinetic energy distribution of tin ions in vacuum is also given in the inset of Fig. 9(a). Ion TOF profile in vacuum is represented by a sharp prompt peak followed by a broad slower peak. The fast prompt peak in the ion signal is caused by photoelectric effect and can be used as a time marker. The estimated expansion velocity of positive ions is ~4.3 $\times 10^6$ cm s^{-1}.

The TOF profiles at 100 mTorr argon showed that most of the ions are quenched before reaching the collector plate. However, as seen in the inset of Fig. 9(b), in the presence of 100 mTorr Ar, the intensity of the prompt peak becomes significantly higher and broadened temporally with large decay time. This is presumably caused by the presence of ambient plasma excited by prompt electrons in the vicinity of the charge collector system. Figure 10 shows the integrated yield of Sn ions as a function of argon pressure. The total yield has been obtained by integrating the area under the ion profile. It

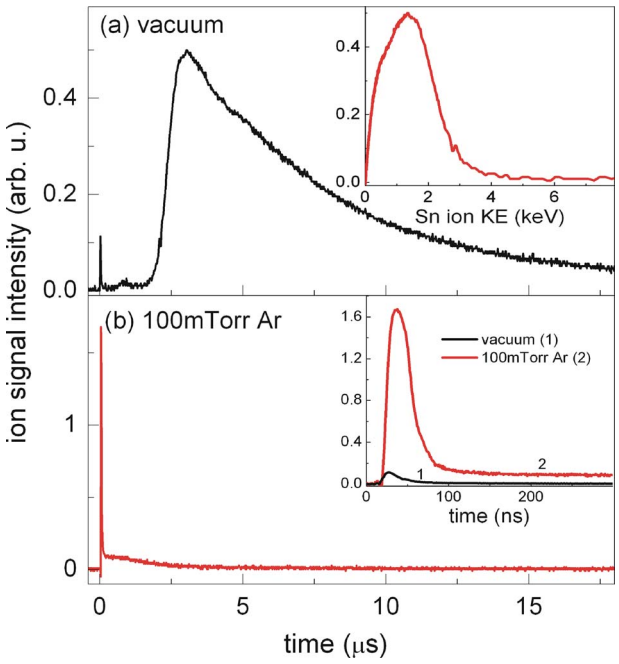

FIG. 9. (Color online) TOF of ions recorded using a Faraday cup placed at a distance ~15 cm from the target surface for plume expansion into vacuum (a) and into 100 mTorr argon pressure (b). The kinetic distribution of the tin ions obtained from TOF signal in vacuum is given in the inset of (a). An enlarged view of the prompt signal observed with vacuum and 100 mTorr Ar is also given in the inset of (b).

provides an indication of mitigation of ion species with increasing buffer gas pressure. The data show that the ion flux reduces rapidly when the ambient pressure increases from 10 to 50 mTorr. It also indicates that approximately 65 mTorr argon pressure is enough for mitigation of tin ions if the collector mirror is placed around ~15 cm from the target surface.

B. Ambient plasma effects

Time of flight spectroscopic studies showed that the faster component of Sn^+ is transmitted through low-pressure argon ambient with little or no delay similar to vacuumlike

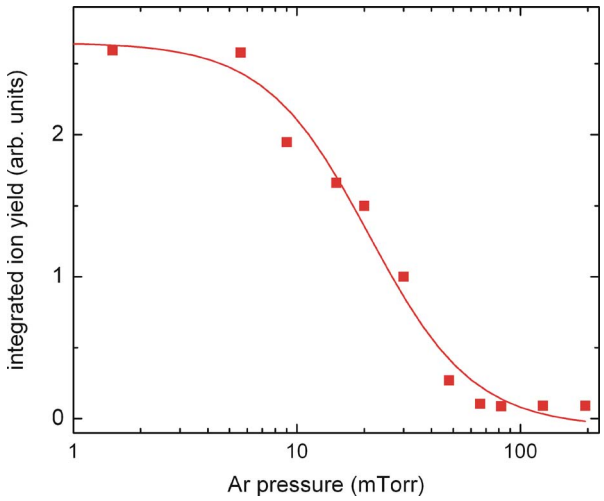

FIG. 10. (Color online) Integrated ion yield obtained from Faraday cup TOF ion data at different argon pressure levels.

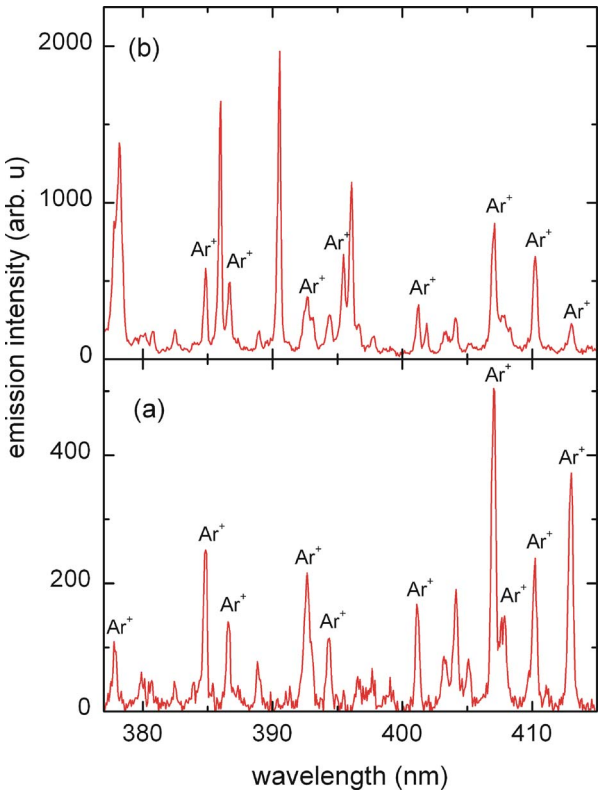

FIG. 11. (Color online) Typical spectrum from tin plasma recorded at 5 mm from the target for different times after the onset of plasma is given. The gate width of the intensifier was 30 ns. (a) Spectra recorded with 0 ns delay time after the arrival of laser pulse and (b) spectra recorded with 200 ns delay time. The emission features at early time showed only lines due to ambient argon plasma.

expansion. This peak existed only within a pressure range of 30–300 mTorr. The exact mechanism for the formation of the faster kinetic peak of Sn^+ in the presence of moderate argon ambient gas is still unclear. TOF profiles of ions recorded using a Faraday cup also showed a large intensity increase in the prompt signal in the presence of 100 mTorr ambient argon even though most of the delayed component was quenched. This may be caused by the presence of ambient plasma. To verify this aspect, optical emission spectroscopic studies of tin plasma in the presence of argon buffer were carried out and it showed strong argon emission lines along with tin line emission. Typical spectra from tin plasma recorded at 5 mm from the target for different times after the onset of plasma are given in Fig. 11. The gating used for recording the spectra was 30 ns and the delays after the onset of plasma formation were 0 ns [Fig. 11(a)] and 200 ns [Fig. 11(b)], respectively. Various emission lines due to argon buffer are marked in the figure. The spectral features showed emission due to singly ionized argon lines that appear even before the arrival of the tin plasma emission at 5 mm. At 5 mm, the tin ionic and atomic lines appear 80 ns after the onset of plasma formation. It indicates that the laser plasma from tin is preceded by partially ionized ambient gas plasma. The argon line emissions also appeared along with tin plasma emission at later times caused by bulk plasma excitation.

To gain more insight, we performed space and time resolved spectral emission studies of argon ions at 480.6 nm

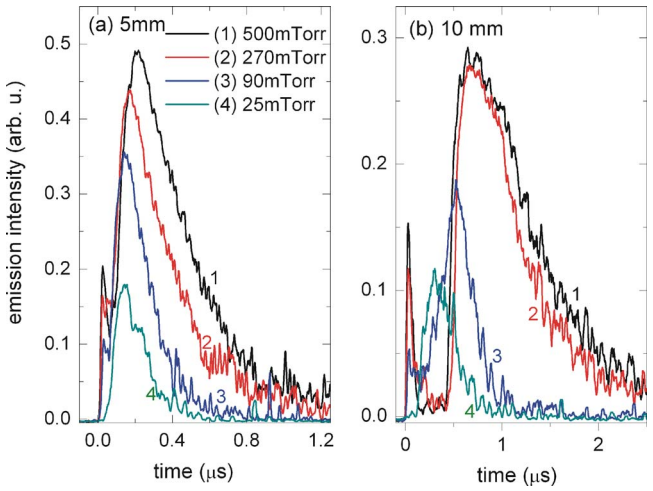

FIG. 12. (Color online) Temporal emission profiles of Ar^+ recorded at distances of 5 and 10 mm from the target for various argon pressures.

($4p\ ^4P_0$-$4s\ ^4P$) at different distances from the target surface. Typical temporal profiles of Ar^+ are given in Fig. 12 recorded at distances of 5 and 10 mm from the target for various argon pressures. Recorded temporal profiles of ionized argon spectral lines exhibited a clear dual peak structure (Fig. 12). The fast peak that appeared instantaneously after the onset of plasma formation (as seen in the spectra) is found to be very narrow (FWHM of 20–35 ns). The slower peak in the argon profile is very broad and caused by bulk plasma excitation. Recently, Saeki *et al.*[49] investigated the excitation mechanisms of buffer gas in a laser ablation process and they noticed similar fast and slow distributions for excited neon and ascribed due to level-selective excitation. The profiles recorded for ambient argon ions showed that the fast temporal peak existed at very early time regardless of the spatial point from the target surface. The faster peak may be caused by argon gas excitation by prompt electrons formed during the early stages of laser ablation. These initial electrons lead to further rapid accumulation of ions and electrons through electron-impact excitation of argon atoms.[50]

To verify the emission of prompt electrons, negatively charged particles were recorded using a Faraday cup. Figure 13 shows the temporal behavior of the electrons obtained with a Faraday cup by biasing it positively. The temporal profiles of negative signals also showed two peaks—a fast kinetic peak, which appeared with very little time delay with respect to the laser pulse (caused by prompt electrons) and a broader peak that coincides with the bulk plasma emission.

The topic of prompt or fast electrons from a laser-produced plasma is an intriguing field of research. These electrons are generated during the interaction of the laser pulse with the target material and possess high kinetic energies. There exists some controversy on the origin of these prompt electrons during a nanosecond laser-matter interaction. Amoruso *et al.*[51] observed highly energetic prompt electrons using an electrostatic energy analyzer (EEA) during excimer laser ablation of an aluminum target and attributed these to two photon photoelectric effects during the laser pulse. Issac *et al.*[52] observed a similar kinetic distribution of fast electrons using a Langmuir probe during Nd:YAG laser

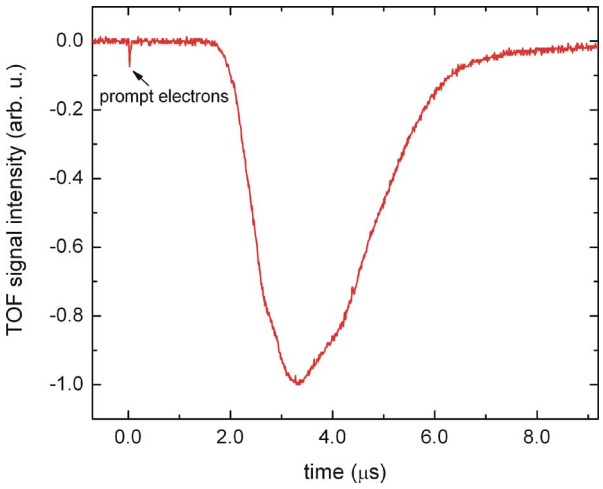

FIG. 13. (Color online) Time of flight profile recorded using a positively biased Faraday cup placed at 15 cm from the target surface. The sharp peak in the early time is due to prompt electrons and the bulk plasma electrons cause the delayed peak.

ablation of silver and attributed the phenomenon to laser heated electrons escaping from the interaction volume before the lattice absorbed the energy. Cronberg *et al.*[53] investigated the fast electrons from laser-produced graphite plasmas using a time of flight spectrometer and suggested that the origin of the high kinetic energies was collisional inverse bremsstrahlung absorption experienced by photoemitted electrons. In nanosecond laser ablation, the electron emission can occur by means of several mechanisms including surface photoelectric effect, volume photoelectric effect, thermionic emission, field emission, plasma formation, etc. Apart from that, the ambient gas species can be ionized by the direct absorption of intense UV and EUV emissions from laser plasma. With an indirect diagnostic tool such as optical emission spectroscopy used in the present experiments, it is very difficult it elucidate the exact mechanism for the formation of prompt electrons. So our aim is limited to the characterization of ambient gas plasma created by prompt electrons and its effect on the expansion dynamics of tin plumes.

The spectral studies showed that most of the ambient plasma line emissions are due to singly ionized argon. The interaction between ambient plasma with the laser created plume is very complex in nature. Recently kinetic modeling studies have been carried out on the interaction between laser-produced lead plasma with argon ambient.[54] There exist several excitation and ionization mechanisms for the creation of argon ions. Since the ionization potential of argon (15.8 eV) is much higher than that of the first ionization potential of Sn (7.3 eV), the ionization of gas atoms by charge transfer is not possible. In fact, the first ionization potential of argon is higher than the second ionization potential of tin (14.6 eV). Moreover, excited argon neutrals possess two metastable levels ($3p\ ^5 4S\ ^3P^0_{0,1}$) and they have high excitation energies (11.6 eV), which can serve as energy reservoirs. Hence the Penning ionization of Sn (i.e., $Ar^* + Sn \rightarrow Ar + Sn^+ + e$) can occur. In the present experiment the ambient plasma precedes the bulk plasma. It is probable that these highly excited argon ions can excite and ionize Sn species.

The ion signal measured with the Faraday cup showed an intense peak with short arrival time followed by the prolonged decay in the presence of ambient gas. This is presumably caused by the presence of ambient plasma excited by prompt electrons in the vicinity of the charge collector system. The prolonged decay time of the sharp peak is due to various lifetimes of excited states involved in the argon ion excitation and ionization. This is supported by the fact that the temporal evolution of prompt electron excited Ar^+ lines (first peak) showed (Fig. 12) broader temporal profiles (FWHM=20–35 ns) in comparison with the prompt electron signal measured with the Faraday cup (Fig. 13). It should be remembered that most of the Ar^+ transitions are characterized by lifetimes ~10–25 ns.[55].

The estimated ion velocity using the Faraday cup showed much higher values (4.3×10^6 cm/s) than the measured expansion velocities of Sn^+ using optical TOF in vacuum (1.8×10^6 cm/s). The higher velocity observed by the Faraday cup may be contributed by highly charged tin ions that are not detectable with visible spectroscopy. This can be understood by considering the plume expansion in the initial stages where electrons strive to overtake the ions resulting in a space charge field that accelerates ions causing higher velocity for highly charged ionic states. It has been reported that ions of the highest ionization state dominate in the direction of maximum emission and that their concentration falls sharply away from the normal.[56] The ions located at the front of the plasma acquire the largest energy during hydrodynamic acceleration and the interaction time for recombination is very much reduced. The addition of ambient gas leads to more efficient electron impact excitation and plasma recombination, which enhances the emission from these species in the plasma. The faster peak of Sn^+ is expected to be contributed by the recombination of highly charged ions in the presence of ambient gas. The faster peak of Sn^+ occurs when the argon pressure is greater than 30 mTorr and this kinetic peak disappears when the pressure is around 300 mTorr. The disappearance of a faster kinetic peak of Sn^+ at higher pressures can be understood by considering the shock wave formation in the plasma-ambient boundary. One of the easiest methods for investigating the hydrodynamics of the plume propagation is using fast photography using an ICCD.[57,58] It provides two-dimensional snap shots of the three-dimensional plume propagation.

Time sequences of two-dimensional (2D) images recorded with an ICCD are given in Fig. 14 for 100 and 300 mTorr argon ambient pressures. The gating time used increased progressively from 2 to 20 ns with an increasing delay after the onset of plasma formation. Plume images obtained with the ICCD show that the plasma becomes more collisional when the ambient gas pressure increases from 100 to 300 mTorr. At 100 mTorr, the plume species diffuse into the ambient gas and no sharp boundary is formed. When we increased the argon pressure to 300 mTorr, a compressed region is formed between the expanding tin plasma and ambient gas. Here the transition to a hydrodynamic regime takes place, with the plume acting as a piston on the surrounding ambient environment. This compressed region moves ahead of the plume and generates a shock wave. It

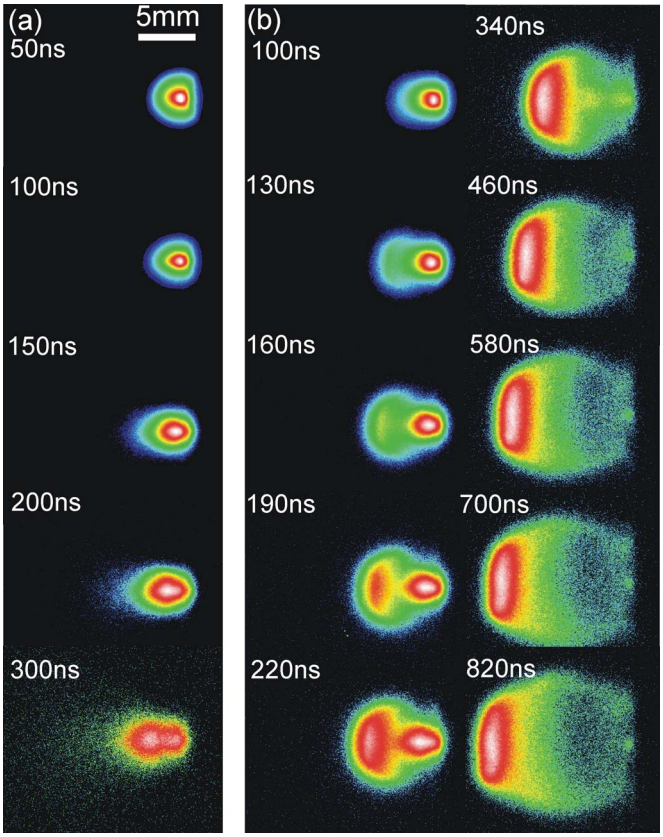

FIG. 14. (Color online) Time sequence of 2D images recorded with a fast-gated ICCD camera is given for tin plasma expansion into 100 mTorr argon pressures (a) and 300 mTorr argon pressure (b). The time noted in the figures corresponding to the time after the onset of plasma formation. Each image is obtained from different laser shots and all the images are normalized to its maximum intensity for better clarity.

also leads to enhance emission from the plume front due to excitation and ionization as a result of transfer of plume kinetic energy into thermal energy (plume heating). The *R-t* behavior of the shock wave is described by[59] $R=\xi_0 (E_0/\rho_0)^{1/5} t^{2/5}$, where ξ_0 is constant related to specific heat capacity (γ), E_0 is the amount of energy released, and ρ_0 is the ambient gas density.[29] In the present case, with 300 mTorr argon pressure the plume followed $R \propto t^{0.43}$ dependence that agrees well with the shock model. When a shock boundary is formed between the plume and ambient gas medium, it effectively shields the diffusion of the ambient gas species from the plasma species. The absence of a faster kinetic peak of Sn^+ above 300 mTorr indicates that the charged ions in the plume front are decelerated and lose their kinetic energy into thermal energy in the plume-ambient boundary.

IV. CONCLUSION

Ion debris mitigation in a laser-produced tin plasma is one of the most important tasks before implementation as an EUVL light source. We attempted to control the Sn ions using an argon buffer. The selection of the inert argon gas is based on the fact that it transmits more than 90% of the in-band radiation centered at 13.5 nm when the pressure is around 100 mTorr. Monte Carlo simulation results showed that with this ambient pressure, the tin species with kinetic energies less than 5 keV could be effectively stopped before reaching the collector mirror in an EUVL source setup. We performed space and time resolved optical emission analysis of various species in the tin plasma to understand the effect of 100 mTorr argon pressures on plume dynamics. Our experimental results have clearly highlighted the influence of ambient argon gas on tin plume kinetics and dynamics even at distances less than 25 mm from the target. Ion TOF profiles and estimated integrated ion yield measurements made with a Faraday cup (FC) placed at larger distances from the target showed that tin ions can be effectively mitigated with a partial argon pressure without significantly influencing the EUV in-band radiation transmission.

The addition of an ambient gas completely changed the hydrodynamics of the plume expansion. Plasma expansion into a vacuum environment is simply adiabatic and expands freely. At 100 mTorr argon, the kinetic distribution of Sn^+ species was transformed into a dual peak structure with the addition of a faster component. The analysis of the time evolution of Sn^+ species shows that the peak splitting effect is observed only beyond a distance of 4 mm from the target in a pressure regime of 30–300 mTorr. This indicates that peak splitting appears at the latter stage of the plume expansion as a consequence of plume-buffer gas interaction. The spectral analysis showed strong emission from the ambient plasma along with tin plume emission.

Time and space resolved studies of ambient argon ions also showed a twin-peak structure. The faster peak, which arrives with a short time delay, was caused by collisional excitation and ionization of the argon species by the prompt electrons ejected during the laser target interaction. A delayed and broad component is also observed and that was excited due to bulk plasma electrons. Although no single piece of data provides decisive proof of the origin of the faster peak of Sn^+, all of the evidences coming from various diagnostic tools used in the present study suggest that the faster Sn^+ peak is formed by the recombination of highly charged tin ions in the presence of ambient gas. The presence of ambient gas leads to more efficient electron-impact excitation and plasma recombination, which enhances the emission from these species in the plasma. The experimental results also show that a combination of various diagnostic tools, viz., optical TOF spectroscopy, ion and electron TOF using a Faraday cup, and ICCD plume imaging, enables us to understand the dynamics of various species in the tin plume at short and large distances from the target surface.

[1] U. Stamm, J. Phys. D **37**, 3244 (2004).
[2] D. W. Myers, I. V. Fomenkov, W. Partlo, D. C. Brandt, and B. C. Klene, Solid State Technol. **48**, 67 (2005).
[3] R. de Bruijn, K. Koshelev, G. Kooijman, E. S. Toma, and F. Bijkerk, J. Quant. Spectrosc. Radiat. Transf. **81**, 97 (2003).
[4] T. Higashiguchi, C. Rajyaguru, S. Kubodera, W. Sasaki, N. Yugami, T. Kikuchi, S. Kawata, and A. Andreev, Appl. Phys. Lett. **86**, 231502 (2005).
[5] Y. Tao *et al.*, Appl. Phys. Lett. **86**, 201501 (2005).
[6] B. Marx, Laser Focus World **39**, 34 (2003).
[7] C. Koay, S. George, K. Takenoshita, R. Bernath, E. Fujiwara, M. Richardson, and V. Bakshi, Proc. SPIE **5751**, 279 (2005).
[8] H. A. Bender, D. Oconnell, and W. T. Silfvast, Appl. Opt. **34**, 6513 (1995).
[9] S. S. Harilal, B. O'Shay, and M. S. Tillack, J. Appl. Phys. **98**, 036102

(2005).
[10]K. Takenoshita, C. S. Koay, S. Teerawattanasook, M. Richardson, and V. Bakshi, Proc. SPIE **5751**, 563 (2005).
[11]S. J. Haney, K. W. Berger, G. D. Kubiak, P. D. Rockett, and J. Hunter, Appl. Opt. **32**, 6934 (1993).
[12]M. Richardson, C. S. Koay, K. Takenoshita, C. Keyser, and M. Al-Rabban, J. Vac. Sci. Technol. B **22**, 785 (2004).
[13]D. B. Chrisey and G. K. Hubler, *Pulsed Laser Deposition of Thin Films* (Wiley, New York, 1994).
[14]A. A. Voevodin, J. G. Jones, and J. S. Zabinski, J. Appl. Phys. **88**, 1088 (2000).
[15]F. Flora, L. Mezi, C. E. Zheng, and F. Bonfigli, Europhys. Lett. **56**, 676 (2001).
[16]S. Bollanti *et al.*, Appl. Phys. B: Lasers Opt. **76**, 277 (2003).
[17]M. W. Stapleton, A. P. McKiernan, and J. P. Mosnier, J. Appl. Phys. **97**, 064904 (2005).
[18]S. I. Anisimov, D. Bauerle, and B. S. Lukyanchuk, Phys. Rev. B **48**, 12076 (1993).
[19]S. I. Anisimov, B. S. Lukyanchuk, and A. Luches, Appl. Surf. Sci. **96–98**, 24 (1996).
[20]R. K. Singh, O. W. Holland, and J. Narayan, J. Appl. Phys. **68**, 233 (1990).
[21]R. K. Singh and J. Narayan, Phys. Rev. B **41**, 8843 (1990).
[22]M. S. Tillack, D. W. Blair, and S. S. Harilal, Nanotechnology **15**, 390 (2004).
[23]A. V. Bulgakov and N. M. Bulgakova, J. Phys. D **31**, 693 (1998).
[24]D. B. Geohegan, in *Pulsed Laser Deposition of Thin Films*, edited by D. B. Chrisey and G. K. Hubler (Wiley, New York, 1994), p. 115.
[25]S. Amoruso, B. Toftmann, J. Schou, R. Velotta, and X. Wang, Thin Solid Films **453–454**, 562 (2004).
[26]T. E. Itina, J. Hermann, P. Delaporte, and M. Sentis, Phys. Rev. E **66**, 066406 (2002).
[27]A. Bogaerts, Z. Y. Chen, R. Gijbels, and A. Vertes, Spectrochim. Acta, Part B **58**, 1867 (2003).
[28]S. S. Harilal, C. V. Bindhu, M. S. Tillack, F. Najmabadi, and A. C. Gaeris, J. Phys. D **35**, 2935 (2002).
[29]S. S. Harilal, C. V. Bindhu, M. S. Tillack, F. Najmabadi, and A. C. Gaeris, J. Appl. Phys. **93**, 2380 (2003).
[30]B. L. Henke, E. M. Gullikson, and J. C. Davis, At. Data Nucl. Data Tables **54**, 181 (1993).
[31]http://www-cxro.lbl.gov/optical_constants/gastrn2.html
[32]J. F. Ziegler, J. Appl. Phys. **85**, 1249 (1999).
[33]http://www.srim.org
[34]J. F. Ziegler, J. P. Biersack, and U. Littmark, *The Stopping and Range of Ions in Solids* (Pergamon, New York, 1985).
[35]S. S. Harilal, B. O'Shay, M. S. Tillack, and M. V. Mathew, J. Appl. Phys. **98**, 013306 (2005).
[36]S. S. Harilal, P. Radhakrishnan, V. P. N. Nampoori, and C. P. G. Vallabhan, Appl. Phys. Lett. **64**, 3377 (1994).
[37]S. S. Harilal, Appl. Surf. Sci. **172**, 103 (2001).
[38]S. S. Harilal, B. O'Shay, Y. Tao, and M. S. Tillack, J. Phys. D **39**, 484 (2006).
[39]S. S. Harilal, M. S. Tillack, B. O'Shay, C. V. Bindhu, and F. Najmabadi, Phys. Rev. E **69**, 026413 (2004).
[40]S. S. Harilal, R. C. Issac, C. V. Bindhu, V. P. N. Nampoori, and C. P. G. Vallabhan, J. Appl. Phys. **81**, 3637 (1997).
[41]W. D. Westwood, J. Vac. Sci. Technol. **15**, 1 (1978).
[42]S. Amoruso, R. Bruzzese, R. Velotta, N. Spinelli, A. Vitiello, and X. Wang, Appl. Surf. Sci. **248**, 45 (2005).
[43]W. O. Siew, K. H. Wong, S. S. Yap, and T. Y. Tou, IEEE Trans. Plasma Sci. **33**, 176 (2005).
[44]S. M. Park and J. Y. Moon, J. Chem. Phys. **109**, 8124 (1998).
[45]T. Kerdja, S. Abdelli, D. Ghobrini, and S. Malek, J. Appl. Phys. **80**, 5365 (1996).
[46]D. B. Geohegan, Appl. Phys. Lett. **60**, 2732 (1992).
[47]D. B. Geohegan and A. A. Puretzky, Appl. Phys. Lett. **67**, 197 (1995).
[48]R. F. Wood, K. R. Chen, J. N. Leboeuf, A. A. Puretzky, and D. B. Geohegan, Phys. Rev. Lett. **79**, 1571 (1997).
[49]M. Saeki, K. Hirata, T. Sakka, H. Ohba, and A. Yokohama, J. Appl. Phys. **98**, 044912 (2005).
[50]R. C. Issac, P. Gopinath, S. S. Harilal, V. P. N. Nampoori, and C. P. G. Vallabhan, Appl. Phys. A: Mater. Sci. Process. **67**, 557 (1998).
[51]S. Amoruso, M. Armenante, R. Bruzzese, N. Spinelli, R. Velotta, and X. Wang, Appl. Phys. Lett. **75**, 7 (1999).
[52]R. C. Issac, P. Gopinath, V. P. N. Nampoori, and C. P. G. Vallabhan, Appl. Phys. Lett. **73**, 163 (1998).
[53]H. Cronberg, M. Reichling, E. Broberg, H. B. Nielsen, E. Matthias, and N. Tolk, Appl. Phys. B: Photophys. Laser Chem. **52**, 155 (1991).
[54]V. I. Babushok, F. C. DeLucia, Jr., P. J. Dagdigian, and A. W. Miziolek, Spectrochim. Acta, Part B **60**, 926 (2005).
[55]S. S. Harilal, Appl. Opt. **43**, 3931 (2004).
[56]A. Thum-Jaeger, B. K. Sinha, and K. P. Rohr, Phys. Rev. E **63**, 016405 (2001).
[57]S. S. Harilal, B. O'Shay, M. S. Tillack, C. V. Bindhu, and F. Najmabadi, IEEE Trans. Plasma Sci. **33**, 474 (2005).
[58]S. S. Harilal, C. V. Bindhu, and H. J. Kunze, J. Appl. Phys. **89**, 4737 (2001).
[59]Y. B. Zel'dovich and Y. P. Raizer, *Physics of Shock Waves and High-Temperature Hydrodynamic Phenomena* (Academic, New York, 1966).